IRnet: Immunotherapy response prediction using pathway knowledge-informed graph neural network

Abstract

Introduction: Immunotherapy, specifically, immune checkpoint inhibitors (ICIs) are powerful and precise therapies for many cancer types and have improved the survival of patients who positively respond to them. However, only a minority of patients respond to ICI treatments.

Objectives: Determining ICI responders before treatment would dramatically save medical resources, avoid potential drug side effects, and save valuable time by exploring alternative therapies. Here, we aim to present a novel deep-learning method that can predict ICI treatment response in cancer patients.

Methods: The proposed deep-learning framework leverages graph neural network and biological pathway knowledge. We trained and tested our method using ICI-treated patients' data from several clinical trials covering melanoma, gastric cancer, and bladder cancer.

Results: The results indicate that the prediction performance is superior to other currently available state-of-the-art methods or tumor microenvironment-based predictions. Moreover, the model quantifies the importance of pathways, pathway interactions, and genes involved in the prediction.

Conclusion: IRnet is a competitive method and tool in predicting patients' response to immunotherapy, specifically immune checkpoint inhibitors (ICI). The interpretability of IRnet provides insights into mechanisms involved in the different ICI treatments.

Keywords: Machine learning, graph neural network, biological pathway, immunotherapy response, checkpoint inhibitors, model interpretability

Introduction

Immunotherapy presents a promising and inventive strategy for addressing cancer, with a notable focus on restraining different immune checkpoint inhibitors (ICIs) that regulate the activity of host T-cells [1]. The interaction between programmed cell death 1 (PD-1) and its ligand PD-L1 has gained prominence as a widely employed mechanism through which cancer cells elude the immune responses launched by the host [2]. Another ICI called cytotoxic T lymphocyte antigen-4 (CTLA-4) was demonstrated to have a strong inhibitory role in regulating T-cell response [3]. Despite the FDA's accelerated approval for newer immunotherapy drugs, the outcome and response to treatments remain dismal in most cancers [4]. Doctors consider several factors when determining if a patient would benefit from immunotherapy, including cancer type [5], cancer stage [6], and the status of biomarkers or tumor micro-environment (TME), which describe the patient heterogeneity directly. These biomarkers include ICI targets, e.g., PD-L1 [7], Microsatellite Instability (MSI) [8], and tumor mutational burden (TMB) [9,10].

Since these have been reported to correlate with immunotherapy response, many computational methods have used them as features and achieved improvements in determining immunotherapy

responders [11–15]. Specifically, Auslander et al. built the immune predictive score (IMPRES) by encompassing 15 pairwise transcriptomics relations between immune checkpoint genes. A predictor that counts the number of fulfilled feature pairs was made to predict melanoma response to ICB [11]. In the TIDE method, Jiang et al. modeled two mechanisms of tumor immune evasion: the induction of T-cell dysfunction in tumors with high infiltration of cytotoxic T lymphocytes (CTL) and the prevention of T-cell infiltration in tumors with low CTL level. The corresponding signatures (T-cell dysfunction and exclusion) were defined using relative gene markers or cell types. And the ICB response prediction is based on the Pearson correlation between patients' transcriptome with either T-cell dysfunction or exclusion signatures [12]. Bagaev et al. classified tumor microenvironment (TME) using knowledge-based functional gene expression signatures representing the major functional components and immune, stromal, and other cellular populations of the tumor. Four conserved TME subtypes were revealed and correlate with immunotherapy response in Melanoma [13]. Two recent works transform gene markers into network markers. Kong et al. applied network propagation using ICI targets as seed genes, then identified pathways enriched with high influence genes [14]. While Zhao et al. used ICI targets (such as PD1 or PD-L1) as anchor nodes to propagate the effects of ICI targets across the network, then selected those pathways with targeted genes related in gene oncology networks and injected these pathways on the gene sets [15]. The derived network markers then used as inputs to machine learning models to predict immunotherapy response. All these methods are based on some pre-selected gene markers, in most cases, ICI targets.

However, some studies reported no significant positive correlation between ICI response and biomarkers such as PD-L1 expression [16,17] or MSI [18]. Some studies have even revealed that ICI responders display low PD-L1 expression levels [19]. This patient heterogeneity partially explained the low response rate in most ICI treated cancers and the failure cases from the existing prediction methods. We argue that the focus on canonical biomarkers by current prediction methods would introduce bias, while some missed features might not be directly related to ICI response, but still be important because of their interactions with other biomarkers or roles in signal transduction. Furthermore, gene-level features used by other ICI response prediction methods are noisy. Several deep-learning applications for other research fields have embedded gene features into pathways or even higher-level features such as biological process [20–23], thus yielding more generalized and robust features and increasing the interpretability of models.

In this paper, we propose IRnet, an interpretable deep-learning framework to predict ICI response, which has several novel features as compared to other existing methods. Firstly, we do not select any biomarkers in advance. The input is the whole genome transcriptome from patients and the model will automatically learn the importance of markers. Secondly, Irnet transforms gene expression into pathway embeddings according to current knowledge and performs a graph neural network at the pathway level. Finally, the model is designed to provide three levels of explanation: pathway importance, pathway interaction importance, and gene importance. We tested IRnet on several immunotherapy clinical trial datasets and found that IRnet outperformed other current state-of-the-art ICI response prediction methods. Besides prediction, the top-ranked pathways and genes are generally consistent with immunotherapy related

findings, further highlighting the relevance of our predictions. We think that this study would eventually be a valuable decision-making reference for clinicians so that both patients and care providers could save time and resources.

Methods

Datasets collecting and processing

The pathway information, including the genes involved in each pathway, and pathway interactions, are extracted from the KEGG database [24] using the KEGG REST API. The patient whole genome transcriptomics data before ICI treatment and the response after treatment were collected from the following immunotherapy clinical trials: for the Liu dataset [25], the gene counts were obtained from the GitHub repository at https://github.com/vanallenlab/schadendorf-pd1 mentioned in the original paper; for datasets of Gide [26] and Kim [27], raw RNA-seq data were obtained from the European Nucleotide Archive (ENA) under the project numbers PRJEB23709 and PRJEB25780, and the gene counts were generated through RNA-seq analysis pipeline (see Methods); for the IMvigor210 [28] dataset, the gene counts was obtained using the easierData R package [29]; for datasets of Auslander [11] and Riaz [30], the gene counts were downloaded from the Gene Expression Omnibus (GEO) [31] under the accession numbers GSE115821 and GSE91061. The patient transcriptomics and survival data in TCGA datasets were downloaded using the TCGAbiolinks R package[32], including the following projects: (i) TFGA SKCM for melanoma; (ii) TCGA STAD for stomach adenocarcinoma; and (iii) TCGA BLCA for bladder cancer. As to the pre-processing of gene expression data, sample-wise z-score is calculated based on gene counts. So that future individual patient data could be processed without relying on the cohort.

We used response evaluation criteria in solid tumors (RECIST) to classify samples into responders and non-responders, as in previous studies [12,14,33–35]. Complete response (CR) and partial response (PR) were classified as responders, while stable disease (SD) and progressive disease (PD) were classified as non-responders, as in previous studies. For datasets that did not provide or use RECIST criteria (Auslander dataset), we used responder and non-responder classification from the original paper. All datasets used in this paper are summarized in the Supplementary Table S5.

RNA-seq data analysis pipeline

Forty-five samples (only the RNA sequencing samples) in Kim dataset and all 91 samples in the Gide dataset from the European Nucleotide Archive (ENA) were downloaded to our server using the wget command with the respective FTP links. All downloaded samples are paired-end RNA sequencing samples in FASTQ format. We checked the quality of those FASTQ files using both Fastqc [36] and MultiQC [37] tools. All the raw reads in the FASTQ files are in decent condition. Furthermore, the raw reads were aligned with the GRCh38 human reference genome using the STAR alignment tool [38]. In the alignment process, the coordinates were sorted automatically to generate Binary Alignment Map (BAM) files. The BAM files of each set were utilized for generating the raw RNA counts using the FeatureCounts tool [39]. In the processes, the GRCh38 human General Feature Format (GFF) files and Gene Transfer Format (GTF) files were used.

IRnet training and predicting strategy

To address the small and imbalanced data issue, we performed bootstrap and transfer learning during the IRnet training. Specifically, we called the StratifiedKFold function in the sklearn package [40] to divide a dataset into 5 folds with similar class ratios. In each StratifiedKFold iteration, 1 fold would be kept out for testing, 80% of samples in the left 4 folds were used as training samples, and the remaining 20% samples for validation. We set the targeting number *N* as two folds of the sample number in the majority class in the training set. We then calculated the sample number differences d_{major} for the majority class and d_{minor} for the minority class compared to *N*. Finally, we randomly sample d_{major} and d_{minor} times with replacement from the majority class and the minority class, respectively, and combined them with the original data in the training folds to complete the bootstrap process. For the transfer learning, three TCGA project data were merged to pre-train IRnet models according to the cancer type of fine-tune data, e.g., SKCM for melanoma, STAD for gastric cancer, and BLCA for bladder cancer. Since TCGA doesn't provide immunotherapy response information, we used patient survival information to pre-train the model and set the survival threshold as 2 years (patients survival less than two years after treatment will be labeled 0, otherwise 1). Thus, IRnet could be evaluated in different configurations (e.g. in Table S1 and Table S2): not using bootstrap or transfer learning (vanilla IRnet); using bootstrap alone; using transfer learning alone; or using both bootstrap and transfer learning, which is also the strategy of the final IRnet model (for comparing with other methods or model interpretation). The model was trained using an Adam optimizer with a learning rate equal to 0.0001. The number of epochs was fixed as 400 and the weights of the epoch with the highest validation F1 score will be saved as the sub-model weight for that 5-fold split. When predicting, five sub-models trained by five StratifiedKFold iterations will run on the targeting samples, and the ensemble of their predicted scores will be used for the final prediction.

We also applied Focal Loss [41] to alleviate the problem of class imbalance because examples from the majority class are usually easy to predict, while those from the minority class are hard due to a lack of data or examples from the majority class dominating the loss and gradient process. Focal loss applies a modulating term to the cross-entropy loss in order to focus learning on hard misclassified examples. It is a dynamically scaled cross-entropy loss, where the scaling factor decays to zero as confidence in the correct class increases. Intuitively, this scaling factor can automatically down-weight the contribution of easy examples during training and rapidly focus the model on hard examples. Formally, the Focal Loss adds a factor $(1 - p_t)^\gamma$ to the standard cross-entropy criterion. Setting $\gamma > 0$ reduces the relative loss for well-classified examples (p_t > 0.5), focusing more on hard, misclassified examples. There is a tunable focusing parameter $\gamma \geq 0$, and the Focal Loss is calculated as the formula below,

$$FL(p_t) = -(1 - p_t)^\gamma \log(p_t)$$

Pathway importance calculation

The pathway importance is valued based on the attention weights in the global attention pooling layer. The attention is calculated following the formula below:

$$att = softmax(XW + b) ,$$

where X is the output tensor from the previous GAT layer, with dimension (batch size, 344, 4). W is the learnable kernel with dimensions (4, 8). b is the bias vector with length 8. The resulting tensor has a dimension equal to (batch size, 344, 8), recording the attention weight of all 344 pathways for each patient in the batch by 8 different channels. To simplify the analysis, we took the average over the patient dimension and channel dimension.

Pathway interaction importance calculation

The pathway interaction importance was measured based on the attention weights from the second GAT layer in the IRnet architecture. The attention between two nodes in a GAT layer is calculated using the formula below:

$$att_{ij} = \frac{\exp\left(LeakyReLU(\alpha^T[W\overrightarrow{h_i}||W\overrightarrow{h_j}])\right)}{\sum_{k\in N_i}\exp\left(LeakyReLU(\alpha^T[W\overrightarrow{h_i}||W\overrightarrow{h_k}])\right)},$$

where $\alpha \in \mathbb{R}^8$ is a trainable attention kernel. $W\overrightarrow{h_i}$ and $W\overrightarrow{h_j}$ are representation vectors with length equals 4 for pathway *i* and *j*, respectively. The resulting attention is a tensor with dimension (batch size, 344, 344). Each patient has his or her attention matrix, which is very sparse and each non-zero element indicates the pathway interaction weight from one pathway to another. By using the softmax function, the derived pathway interaction weight from pathway *j* to pathway *i* is the relative importance of pathway *j* among all the neighbor pathways of pathway *i*.

Gene importance calculation

The gene importance was measured based on the learned weights of the FFN layer that mimic the gene to pathway memberships. Unlike the pathway or pathway interaction importance, which are patient specific, gene importance (the weights) is fixed once the IRnet model is trained. The FFN is fully connected, while the biological fact it represents is very sparse. One gene could only work in one or several pathways. In total, there are 33,170 non-zero elements in the matrix, indicating the gene importance in different pathways, while the maximum possible number is 2,779,520 (8080 genes times 344 pathways).

Statistical analysis

For the survival analysis, we used Kaplan-Meier estimator [42] to estimate the survival function with the right-censored overall survival data. To measure the performance of survival models, we calculated the Harrell's concordance index or c-index [43]. The interpretation is identical to the traditional area under the ROC curve metric for binary classification: a value of 0.5 denotes a random model, a value of 1.0 denotes a perfect model, a value of 0.0 denotes a perfectly wrong model. In order to assess whether there is a difference in survival between groups, we performed the log-rank test to calculate p-values. To test the significance of the averaged percentile of TME-associate markers, as well as the significance of the ratio of top-ranked pathways connected by the top-ranked pathway interactions, we calculated the p-values by running empirical Monte Carlo simulations. Specifically, we randomly chose the same number of genes for each TME-associate marker and calculated its average percentile. We repeated this process 1000 times and checked how many times the randomly calculated score is equal or greater than the averaged percentile of real TME-associate markers. Similarly, to calculate the p-value of the ratio of top-ranked

pathways in top interactions, we randomly selected 30 pathways and up to 3 connecting pathways for each. Then, we calculated the ratio of the random pathways in the resulting graph. We also repeated this process 1000 times and checked how many times the ratio is equal or greater than the top pathway ratio in the top-ranked interactions.

Results

IRnet framework overview

The IRnet framework and its workflow are presented in Figure 1. According to current knowledge, three types of data were collected, including whole genome transcriptomics data from ICI clinical trial patients before treatment, pathway relationships, and gene membership in those pathways. During the training, all three types of data were needed, among which the pathway relationships and gene memberships were embedded as part of the model architecture. Thus, the transcriptomics data is the only information needed during the prediction phase.

The architecture of IRnet is mainly divided into three parts, each designed to provide explanation at the corresponding level. The first part is a fully connected feed-forward layer between genes and pathways but masked according to gene membership. Specifically, 8080 genes are connected to 344 KEGG pathways via 33,170 links (a gene is linked to a pathway if that gene is involved in the pathway, KEGG release 105.0). The number of genes is lower than the whole genome, as the genes with no pathway details due to the incomplete knowledge of KEGG pathways are omitted. The pathway embeddings are obtained as tanh function-activated weighted sum of gene expression (normalized). And the learned weights represent the importance of genes. The second part is a multi-head graph attention network (GAT) [44] using the pathway embeddings as inputs. The graph contains 344 nodes and 3152 edges. Each node represents a KEGG pathway, and the edges indicate their interactions (defined as “related pathway” in the KEGG database). During the training phase, the embedding of each pathway is updated through the message passing from its neighbor pathways. We stacked two GAT layers. Both of these set the dimension of pathway embedding vector as 4. The first GAT has three attention heads, while the second GAT has only one head for edge attention weights and is learned to capture the pathway interaction importance. In the last part of IRnet, we utilized a global attention pooling [45] to obtain the representation of the entire pathway graph. Essentially, it is an element-wise multiplication between a feature feedforward neural network (FFN) and an attention FFN. Both have the channel number as 8. We extracted the attention outputs and used them to rank the pathway importance. The global attention pooing layer is followed by a fully connected FFN, which leads to final predictions.

There are two main challenges in training IRnet for ICI response prediction. One is the lack of patient samples. It is difficult to train a deep learning model with several hundreds of samples, and the sample numbers get even smaller if treating different immunotherapy clinical trials individually. The second challenge resides in the nature of the ICI treatment is that the response rate is low, causing imbalanced training data. To mitigate the first issue, we utilized the patient transcriptomics data and survival information in The Cancer Genome Atlas (TCGA). We found a correlation between ICI response and survival time, as

indicated in Supplementary Figure S1. Based on this, we pre-trained IRnet using TCGA data and survival time as labels, then fine-tuned it with ICI data as a typical strategy in transfer learning to increase training samples. To address the training sample imbalance issue, we performed bootstrapping to resample the data from the minority class. The details of IRnet training strategy are described in the Methods section.

Within-cohort validation

In the experimental setting of within-cohort, methods were trained and tested on samples from the same immunotherapy dataset. We evaluated the performance of IRnet in predicting ICI response by cross-validation within each dataset. For each immunotherapy clinical trial dataset, we split it into five folds and kept the ratio of responder to non-responder in each fold similar. A five-fold cross-validation was performed and the mean of different scores was reported (see details of IRnet training and testing in the Methods section). The results of within-cohort cross-validation under different experiment configurations are shown in Supplementary Table S1. According to the results, using bootstrap or transfer learning alone did improve the performance compared to the vanilla model, while using both strategies achieved the best performance in most of the datasets. We also compared the IRnet performance with other methods, including NetBio, GeneBio, and TME-Bio [14], which are regression methods based on network-based biomarkers (NetBio), gene-based biomarkers (GeneBio), and tumor microenvironment-based markers (TME-Bio), respectively. The within-cohort performance of these methods was directly cited from the original paper [14]. The comparison results are shown in Figure 2. Among the four immunotherapy datasets we tested, IRnet achieved the best performance in three of them, but not in the Liu dataset, where the NetBio method performed better. Also note that the other three methods were validated by leave-one-out cross validation instead of 5-fold cross validation.

Cross-cohort validation

Further, we evaluated the IRnet performance in cross-cohort scenario. That means training IRnet using one immunotherapy dataset, and then testing it using another independent dataset. We showed the cross-cohort validation results in Supplementary Table S2, where IRnet was trained using the Gide or Liu dataset (both are melanoma), and tested on Riaz (melanoma), Auslander (melanoma), IMvigor210 (bladder cancer), or Kim (gastric cancer) datasets. The cross of training and testing covers different cancer types and different ICI treatment cases. Similar to the within-cohort validation, the results in Table S2 are also shown by different training strategies. In addition, a consistent conclusion is observed in the cross-cohort experiment, that is, using both bootstrap and transfer learning benefits the performance most in the majority of the datasets. We also noticed that the prediction performance on the IMvigor dataset declined compared to the IMvigor performance in Table S1, either trained by the Gide or Liu dataset. Since the Gide and Liu datasets are all melanoma, while IMvigor210 is a bladder cancer dataset, it appears that cancer type plays a role in determining ICI response based on features unique to the specific cancer. Furthermore, patients in the Gide dataset were treated with anti-PD-1 (Nivolumab and pembrolizumab) alone or combined with anti-CTLA4 (Ipilimumab), and patients in the Liu dataset were treated with anti-PD-1 (Nivolumab and pembrolizumab) alone. While in the IMvigor210 datasets, patients were treated with anti-PD-L1

(Atezolizumab). Thus, we believe that the difference in ICI treatment between the training and testing datasets is another factor that harms the prediction performance. Our conclusion is further validated through the prediction results on the Auslander dataset, as shown in Table S2. The patients in the Auslander dataset have melanoma and were treated with anti-PD-1 or anti-CTLA4. When predicting these patients' ICI response, IRnet trained by the Gide dataset has a much better performance than the IRnet model trained by the Liu dataset, in which the patients were only treated with anti-PD-1.

We then compared the IRnet with other state-of-the-art methods in the cross-cohort prediction setting. Besides the methods compared in the within-cohort experiment, we also compared with Tide [12], and showed the comparison results in Figure 3. IRnet achieved the best or most competitive performance on most datasets except for the IMvigor dataset due to the cancer and treatment differences. In the first rows in Figure 3 (A)(B), the performance of NetBio, GeneBio, and TME-Bio was directly cited as claimed in the original paper [14]. In the other datasets, we implemented the NetBio methods but not for GeneBio or TME-Bio because the code is unavailable. Tide method was implemented on all datasets. However, since the training code for Tide is unavailable, we directly applied Tide for prediction. Thus, the tide scores for the same test dataset between Figure 3 (A) and (B) are the same.

We also trained IRnet models by combing several datasets and tested them on the left out independent dataset. It can be regarded as a leave-one-out validation at dataset level and the experiment configurations are shown in Table S3. After comparing with the cross-cohort performance (trained using either Liu dataset or Gide dataset in Table S3), we found that training IRnet using more samples doesn't always yield better performance. The patient samples in different cohorts have different cancer types, ICI treatment, sequencing techniques, even the same ICI treatment could use different drugs. Thus, combining different datasets caused severe batch effect and harms the predictive power of the models.

Immunotherapy response mechanism insight powered by model interpretability

Besides prediction, model interpretability is getting more important in deep-learning applications in many research fields. Not only does the model have potential practical value, but it also increases confidence in the predicted results. IRnet was designed with multiple levels of interpretability, including pathway importance, pathway interaction contribution, and gene relevance. Here, we present the explanations of the results findings from various angles using trained IRnet models.

Pathway importance in ICI response

One unique feature of IRnet method is its pathway-oriented deep-learning architecture. We ranked the pathways based on their importance in ICI response prediction and validated whether the top ranked pathways are related to immunotherapy. The pathway importance was valued by extracting the attention weights in the global attention pooling layer in the IRnet model (see Methods section for details). As indicated by the results in Tables S1 and S2, different ICI treatments affect the immunotherapy response prediction and likely have different mechanisms in fighting cancer. Thus, the pathway importance analysis and other model interpretation analyses were performed in an ICI type-specific way. Three IRnet models were trained using the Liu dataset, Gide dataset, or IMvigor210 dataset for anti-PD1, anti-CTLA4, and anti-

PD-L1, respectively. The learned pathway attention weights ordered from high to low were plotted in Figure S2. For each ICI treatment, we extracted the top 30 ranked pathways to analyze. The information on these three sets of pathways is listed in Supplementary Table S4. And the whole lists of pathway attention weights in three ICI treatments can be accessed in the Supplementary Data.

Many of the top-ranked pathways by IRnet are confirmed to be related to immunotherapy. The overlap of the top ranked pathways from different models and the enriched KEGG pathway categories are shown in Figure 4(A). Among the 19 common pathways between all three ICI treatments, pathways are enriched in KEGG pathway categories, including amino acid metabolism, energy metabolism, metabolism of cofactors and vitamins, and carbohydrate metabolism. Metabolic dysregulation is now recognized as one of the hallmarks of human cancer [46,47] and several studies have explored the impact of metabolic pathways on immune cell function and response to immunotherapy. For amino acid metabolism, particularly certain essential amino acids, have been found to play important roles in immune cell function and response. For example, the availability of amino acids such as tryptophan and arginine can affect immune cell proliferation, differentiation, and effector functions. Perturbations in amino acid metabolism, including alterations in the expression or activity of amino acid transporters or enzymes, can influence immune cell responses and potentially impact the efficacy of immunotherapy [48,49]. Energy Metabolism provides the energy required for immune cell activation and function in the form of ATP.

Studies have shown that manipulating immune cell metabolism, such as inhibiting certain metabolic pathways or providing specific nutrients, can affect immune cell function and alter responses to immunotherapy [50,51]. The metabolism of vitamins, such as vitamin D, vitamin A, and vitamin C, has been found to modulate immune cell function and response. For example, vitamin D has been shown to influence T-cell differentiation and cytokine production, while vitamin A plays a role in regulating immune cell trafficking and mucosal immunity. Deficiencies in specific vitamins can impair immune responses and potentially affect the effectiveness of immunotherapy [52]. As to carbohydrate metabolism, glucose metabolism and other carbohydrate-related pathways have been implicated in immune cell activation and function. Activated immune cells, such as T cells, undergo metabolic reprogramming characterized by increased glucose uptake and utilization. Disruptions in glucose metabolism or alterations in other carbohydrate-related pathways can influence immune cell function and may impact the response to immunotherapy [49]. Besides metabolism-related pathways, ferroptosis is another common pathway that belongs to the cell growth and death category in KEGG. Ferroptosis is a form of regulated cell death implicated in the response to immunotherapy and immune checkpoint inhibitors. Combined ICIs with ferroptosis inducers effectively enhance antitumor immunotherapy, whereas induction of ferroptosis could impair T-cell activity or survival, suggesting that rational combined therapy for cancer is essential [53].

We then analyzed the unique top-ranked pathways in each ICI treatment. Among the eight unique pathways in anti-PD1 treatment, the covered KEGG categories include: 1) cell growth and death (necroptosis), the emergence of a proficient immune profile for necroptosis has important implications for cancer because resistance to apoptosis is one of the major hallmarks of tumors [54]; 2) digestive system

(mineral and protein digestion and absorption), there are researches reported that microbial mechanism and diet-gut microbial interactions improve immune checkpoint blockade responsiveness [55,56]. It involves the digestion and absorption of nutrients and minerals of the host; 3) viral and bacterial infectious disease, which can detrimentally impact the efficacy of cancer immunotherapies [57,58]. It has been reported that signaling through PD-1 results in T-cell apoptosis, exhaustion, and/or anergy, et al., which mediate the downstream events that culminate in activation through the T-cell receptor [59]. This indicates that the unique top-ranked pathways in anti-PD1 treatment found by IRnet are not only related to ICI response but also specific to PD1 signaling. Similarly, in the unique pathways in anti-PDL1, lysine metabolism is involved in PDL1 degradation [60], and pentose phosphate pathway has a critical role in promoting cell survival that increased by PDL1 stimulation [61]. As to the unique pathways founded in anti-CTLA4, it has been proposed that endocytosis of CTLA4 could be inhibited by phenylalanine metabolism, facilitating interactions with ligands that potentially deliver inhibitory signals [62,63]. These findings and supportively literature evidence highlight the importance of the IRnet methods results.

Important pathway interactions link ICI regulators as well as indirectly related pathways

For the pathways that contain the ICI targets, we analyzed the pathways that interact with them and sorted them as per the IRnet ranking (Fig. 4 (B) to (D)). For the pathways where PD1 and PDL1 work, IRnet assigns high pathway interaction weights to immune disease related pathways, e.g. Systemic lupus erythematosus (SLE, hsa05322) and Graft-versus-host disease (GVHD, hsa05332). PD1 and its ligands have been identified in the pathogenesis and development of SLE and GVHD. And some regulators in these disease also regulate the activity of immunobiology [64,65]. The CTLA4 pathway uniquely interacts with other immune system pathways with high IRnet weights, e.g. Antigen processing and presentation (hsa04612), B cell receptor signaling pathway (hsa04662), and Th17 cell differentiation (hsa04659) et al. The role of the biochemical pathway of antigen presentation in cancer has been reviewed in which they discussed how it can be modulated to enhance the efficacy of cancer immunotherapy [66]. Similarly, a review also discussed how ICI therapy impacts Th17 and vice versa [67]. There are also evidence show that CTLA-4 regulation of B cells is a crucial immune-regulatory mechanism[68]. These analyses show that the higher weighted pathway interactions by IRnet could link to ICI related pathways that are patient- and treatment-specific. This could potentially provide insight into ICI response volatility.

Among the top ranked pathways detected in previous section, we also found pathways that are unrelated or not specific to Immunotherapy response. We suspect that these pathways were considered important because of their interaction with immunotherapy response-related pathways. To validate that, we extract the top 3 ranked interactions (see the Methods section for pathway interaction weighting details) for each of the top 30 ranked pathways from each ICI treatment-specific IRnet model. We found that the pathways connected by the top-ranked interactions are enriched in the top ranked pathways as shown in Fig 4 (B) to (D). Among the pathways connected by the top-ranked interactions, we calculated the percentage of the top ranked pathways. The percentage is 51% for anti-PD1 model (p-value<0.001), 72% for anti-PDL1 model (p-value<0.001), and 58% for anti-CTLA4 model (p-value<0.001). This indicates that the top pathways

highly interact with each other. Even though some pathways have not been directly identified to be related to immunotherapy response, they might still be important in signal transduction through pathway interactions.

Highly weighted gene enriched in TME-associated markers

Tumor microenvironment is crucial to immunotherapy [12,69,70]. IRnet model can weigh gene importance from the learned weights in the FFN layer from genes to pathways. We validated the highly weighted genes by checking the average weights of genes in TME markers and calculating the average percentile in the distribution of all gene weights. TME are broadly populated with immune cells, which plays a critical role in response to ICIs [71]. In our study, we chose to check CD8 T cells (T infiltrate), T-cell exhaustion, cancer associated fibroblast (CAFs), and tumor-associated macrophages (TAMs, specifically, M2 macrophages) as TME markers to investigate the correlation between our models. As shown in Figure 5, the averaged weights of TME marker weights are high. Moreover, in the order of T infiltrate, T-cell exhaustion, CAFs, and TAMs, the averaged percentiles are 88th (p-value=0.185), 86th (p-value=0.010), 97th (p-value<0.001), 85th (p-value=0.05) in the anti-PD1 model; 94th (p-value=0.010), 89th (p-value<0.001), 99th (p-value<0.001) , and 85th (p-value=0.005) in the anti-PDL1 model; 92th (p-value=0.040), 93th (p-value<0.001), 88th (p-value=0.565), and 83th (p-value=0.117) in the anti-CTLA4 model. This indicates that T-cell infiltration is represented by the highly weighted genes in the anti-PDL1 and anti-CTLA4 models; both CAFs and TAMs are represented in the anti-PD1 and anti-PDL1 models; and T-cell exhaustion is represented by all three models. The TME markers and highly weighted genes (with a weight percentile>95th) are listed in the Supplementary Data.

Survival analysis based on IRnet ICI response prediction

Finally, we validated whether the IRnet predictions correlate with patient survival. We tested on patient samples in the Gide dataset where matched survival information was available. Besides the whole datasets, we also grouped the patients according to the ICI treatment and did the survival analysis. The results are shown in Figure 6. We found that the patients who were predicted as responders survived significantly longer than non-responders. Quantitively, we used Harrell's concordance index (see Methods section for details) to measure the performance of IRnet survival model. The scores for the whole dataset, the combination of anti-PD1 and anti-CTLA4 treatment patients, and the anti-PD1 treatment patients are 0.641, 0.558, and 0.674, respectively. Moreover, we used log-rank test to assess whether there is a difference in survival between predicted groups. In the same order as the Harrell's concordance index, the log-rank test p-values are 5.02E-4, 0.376, and 7.71E-4.

Discussion

In this work, we developed an interpretable deep-learning framework called IRnet to predict ICI response. Unlike other methods in this field, which predict based on gene-level features, or derive gene sets (pathways)-level features through top-ranked genes and preset gene targets, IRnet is a pathway-centric method that directly transforms gene feature into pathway feature by utilizing current pathway knowledge. We have shown that higher level feature, such as pathway is more robust and less affected by noise than

gene-level features. Though other knowledge-informed methods have been developed, the most significant difference is that IRnet does not preset any target genes, for example, the immunotherapy target genes or TME markers, and the knowledge that IRnet utilizes is generic without the need for it to be ICI-specific. It takes the whole genome transcriptome as input and learns their importance, which is the least affected by subjective bias and has the possibility to discover new markers based on data.

On several benchmark datasets, we demonstrated that IRnet has better or more competitive performance in ICI response prediction than the state-of-the-art methods, either in within-cohort or cross-cohort settings (Figures 2 and 3). We also showed the effectiveness of bootstrap and transfer-learning strategies in addressing imbalanced and minor data issues, leading to a better prediction performance (Tables S1 and S2).

Besides prediction, IRnet provide explanations regarding the results at different levels. The top-ranked pathways are enriched in categories such as metabolism, cell growth and death, digestion and absorption of nutrients and minerals, and viral and bacterial infection. They all have been reported to be related to immunotherapy efficiency. The highly weighted pathway interactions from ICI pathways lead to treatment-specific ICI regulators. Several unrelated pathways were picked among the top-ranked pathways. However, they closely interact with related pathways via the top-ranked pathway interactions (Figure 4). Through the hypotheses test, we found that this phenomenon is not by chance. Some pathways may have a role in immunotherapy response as an intermediate through pathway interactions, but they are not directly related. At gene level, we checked the averaged percentile of weights of TME-associated markers. Hypotheses testing results showed that these makers' weights are significantly skewed in the distribution (Figure 5), indicating IRnet assigned high weights to genes related to TME, which is crucial to immunotherapy response. The model interpretability indicates that IRnet captures the biological mechanism of immunotherapy response, which increases the confidence in the IRnet prediction.

There are also limitations and room to improve the current methods. The biggest bottleneck is the status of publicly available patient data for immunotherapy studies. Most datasets available only release gene expression data. Ideally, raw sequencing data should be made accessible to obtain other relevant information, such as SNP and CNV, as additional features. Furthermore, the data size of immunotherapy datasets is small. Combining all the datasets (even counting the restricted datasets that are inaccessible) only results in a few hundred patient samples with strong batch effects. This undermines the power of deep learning and partially explains why all the state-of-the-art methods are regression-based. In the long term, as more and more ICI-treated patient data is accumulated and available, we believe that the performance of IRnet will further increase.

Conclusions

In conclusion, we have presented an interpretable deep-learning framework to predict patients' response to immune checkpoint inhibitor treatments. This work may play a role in immunotherapy decision making and insights into mechanisms involved in the different ICI treatments.

Code availability

The source codes and a command-line tool for IRnet are available at a GitHub repository (https://github.com/yuexujiang/IRnet). The instructions and an example dataset to predict immunotherapy response using the IRnet tool are provided.

Credit author statement

T.J. supervised the project, involved in results discussion and data collection. Y.J. designed the neural network, developed the code, wrote the manuscript. D.W. helped with neural network tuning and result evaluation, drew some of the figures. S.Z. worked on benchmarking other methods. Y.C worked on RNAseq data processing. J.Z helped with biological background statement. D.X. was involved in method development and overall paper organization.

Acknowledgements

This work is supported by Missouri Department of Health and Senior Services (MDHSS) - Contract #AOC23380006, National Science Foundation (NSF) Cybersecurity Innovation OAC-2232889; and the National Institutes of Health (grant R35GM126985).

The results published here are in whole or part based upon data generated by the TCGA Research Network: https://www.cancer.gov/tcga.

Appendix A. Supplementary material

Supplementary file

Supplementary data

References

[1] Nowicki TS, Hu-Lieskovan S, Ribas A. Mechanisms of Resistance to PD-1 and PD-L1 Blockade. Cancer J 2018;24:47–53. https://doi.org/10.1097/PPO.0000000000000303.

[2] Pardoll DM. The blockade of immune checkpoints in cancer immunotherapy. Nat Rev Cancer 2012;12:252–64. https://doi.org/10.1038/nrc3239.

[3] Ribas A, Wolchok JD. Cancer immunotherapy using checkpoint blockade. Science 2018;359:1350–5. https://doi.org/10.1126/science.aar4060.

[4] Sharma P, Goswami S, Raychaudhuri D, Siddiqui BA, Singh P, Nagarajan A, et al. Immune checkpoint therapy—current perspectives and future directions. Cell 2023;186:1652–69. https://doi.org/10.1016/j.cell.2023.03.006.

[5] Nixon NA, Blais N, Ernst S, Kollmannsberger C, Bebb G, Butler M, et al. Current Landscape of Immunotherapy in the Treatment of Solid Tumours, with Future Opportunities and Challenges. Current Oncology 2018;25:373–84. https://doi.org/10.3747/co.25.3840.

[6] Gridelli C, Rossi A, Carbone DP, Guarize J, Karachaliou N, Mok T, et al. Non-small-cell lung cancer. Nat Rev Dis Primers 2015;1:15009. https://doi.org/10.1038/nrdp.2015.9.

[7] written on behalf of AME Lung Cancer Collaborative Group, Xu Y, Wan B, Chen X, Zhan P, Zhao Y, et al. The association of PD-L1 expression with the efficacy of anti-PD-1/PD-L1 immunotherapy and survival of non-small cell lung cancer patients: a meta-analysis of randomized controlled trials. Transl Lung Cancer Res 2019;8:413–28. https://doi.org/10.21037/tlcr.2019.08.09.

[8] Xiao Y, Freeman GJ. The Microsatellite Instable Subset of Colorectal Cancer Is a Particularly Good Candidate for Checkpoint Blockade Immunotherapy. Cancer Discovery 2015;5:16–8. https://doi.org/10.1158/2159-8290.CD-14-1397.
[9] Strickler JH, Hanks BA, Khasraw M. Tumor Mutational Burden as a Predictor of Immunotherapy Response: Is More Always Better? Clinical Cancer Research 2021;27:1236–41. https://doi.org/10.1158/1078-0432.CCR-20-3054.
[10] Marabelle A, Fakih M, Lopez J, Shah M, Shapira-Frommer R, Nakagawa K, et al. Association of tumour mutational burden with outcomes in patients with advanced solid tumours treated with pembrolizumab: prospective biomarker analysis of the multicohort, open-label, phase 2 KEYNOTE-158 study. The Lancet Oncology 2020;21:1353–65. https://doi.org/10.1016/S1470-2045(20)30445-9.
[11] Auslander N, Zhang G, Lee JS, Frederick DT, Miao B, Moll T, et al. Robust prediction of response to immune checkpoint blockade therapy in metastatic melanoma. Nat Med 2018;24:1545–9. https://doi.org/10.1038/s41591-018-0157-9.
[12] Jiang P, Gu S, Pan D, Fu J, Sahu A, Hu X, et al. Signatures of T cell dysfunction and exclusion predict cancer immunotherapy response. Nat Med 2018;24:1550–8. https://doi.org/10.1038/s41591-018-0136-1.
[13] Bagaev A, Kotlov N, Nomie K, Svekolkin V, Gafurov A, Isaeva O, et al. Conserved pan-cancer microenvironment subtypes predict response to immunotherapy. Cancer Cell 2021;39:845-865.e7. https://doi.org/10.1016/j.ccell.2021.04.014.
[14] Kong J, Ha D, Lee J, Kim I, Park M, Im S-H, et al. Network-based machine learning approach to predict immunotherapy response in cancer patients. Nat Commun 2022;13:3703. https://doi.org/10.1038/s41467-022-31535-6.
[15] Zhao L, Qi X, Chen Y, Qiao Y, Bu D, Wu Y, et al. Biological knowledge graph-guided investigation of immune therapy response in cancer with graph neural network. Briefings in Bioinformatics 2023:bbad023. https://doi.org/10.1093/bib/bbad023.
[16] Brahmer J, Reckamp KL, Baas P, Crinò L, Eberhardt WEE, Poddubskaya E, et al. Nivolumab versus Docetaxel in Advanced Squamous-Cell Non–Small-Cell Lung Cancer. N Engl J Med 2015;373:123–35. https://doi.org/10.1056/NEJMoa1504627.
[17] Carbone DP, Reck M, Paz-Ares L, Creelan B, Horn L, Steins M, et al. First-Line Nivolumab in Stage IV or Recurrent Non–Small-Cell Lung Cancer. N Engl J Med 2017;376:2415–26. https://doi.org/10.1056/NEJMoa1613493.
[18] Rizzo A, Ricci AD, Brandi G. PD-L1, TMB, MSI, and Other Predictors of Response to Immune Checkpoint Inhibitors in Biliary Tract Cancer. Cancers 2021;13:558. https://doi.org/10.3390/cancers13030558.
[19] Bai R, Lv Z, Xu D, Cui J. Predictive biomarkers for cancer immunotherapy with immune checkpoint inhibitors. Biomark Res 2020;8:34. https://doi.org/10.1186/s40364-020-00209-0.
[20] Oh JH, Choi W, Ko E, Kang M, Tannenbaum A, Deasy JO. PathCNN: interpretable convolutional neural networks for survival prediction and pathway analysis applied to glioblastoma. Bioinformatics 2021;37:i443–50. https://doi.org/10.1093/bioinformatics/btab285.
[21] Gut G, Stark SG, Rätsch G, Davidson NR. pmVAE: Learning Interpretable Single-Cell Representations with Pathway Modules. Bioinformatics; 2021. https://doi.org/10.1101/2021.01.28.428664.
[22] Seninge L, Anastopoulos I, Ding H, Stuart J. VEGA is an interpretable generative model for inferring biological network activity in single-cell transcriptomics. Nat Commun 2021;12:5684. https://doi.org/10.1038/s41467-021-26017-0.
[23] Elmarakeby HA, Hwang J, Arafeh R, Crowdis J, Gang S, Liu D, et al. Biologically informed deep neural network for prostate cancer discovery. Nature 2021;598:348–52. https://doi.org/10.1038/s41586-021-03922-4.

[24] Kanehisa M. KEGG: Kyoto Encyclopedia of Genes and Genomes. Nucleic Acids Research 2000;28:27–30. https://doi.org/10.1093/nar/28.1.27.
[25] Liu D, Schilling B, Liu D, Sucker A, Livingstone E, Jerby-Arnon L, et al. Integrative molecular and clinical modeling of clinical outcomes to PD1 blockade in patients with metastatic melanoma. Nat Med 2019;25:1916–27. https://doi.org/10.1038/s41591-019-0654-5.
[26] Gide TN, Quek C, Menzies AM, Tasker AT, Shang P, Holst J, et al. Distinct Immune Cell Populations Define Response to Anti-PD-1 Monotherapy and Anti-PD-1/Anti-CTLA-4 Combined Therapy. Cancer Cell 2019;35:238-255.e6. https://doi.org/10.1016/j.ccell.2019.01.003.
[27] Kim ST, Cristescu R, Bass AJ, Kim K-M, Odegaard JI, Kim K, et al. Comprehensive molecular characterization of clinical responses to PD-1 inhibition in metastatic gastric cancer. Nat Med 2018;24:1449–58. https://doi.org/10.1038/s41591-018-0101-z.
[28] Mariathasan S, Turley SJ, Nickles D, Castiglioni A, Yuen K, Wang Y, et al. TGFβ attenuates tumour response to PD-L1 blockade by contributing to exclusion of T cells. Nature 2018;554:544–8. https://doi.org/10.1038/nature25501.
[29] Lapuente-Santana Ó, Van Genderen M, Hilbers PAJ, Finotello F, Eduati F. Interpretable systems biomarkers predict response to immune-checkpoint inhibitors. Patterns 2021;2:100293. https://doi.org/10.1016/j.patter.2021.100293.
[30] Riaz N, Havel JJ, Makarov V, Desrichard A, Urba WJ, Sims JS, et al. Tumor and Microenvironment Evolution during Immunotherapy with Nivolumab. Cell 2017;171:934-949.e16. https://doi.org/10.1016/j.cell.2017.09.028.
[31] Edgar R. Gene Expression Omnibus: NCBI gene expression and hybridization array data repository. Nucleic Acids Research 2002;30:207–10. https://doi.org/10.1093/nar/30.1.207.
[32] Colaprico A, Silva TC, Olsen C, Garofano L, Cava C, Garolini D, et al. TCGAbiolinks: an R/Bioconductor package for integrative analysis of TCGA data. Nucleic Acids Research 2016;44:e71–e71. https://doi.org/10.1093/nar/gkv1507.
[33] Sakellaropoulos T, Vougas K, Narang S, Koinis F, Kotsinas A, Polyzos A, et al. A Deep Learning Framework for Predicting Response to Therapy in Cancer. Cell Reports 2019;29:3367-3373.e4. https://doi.org/10.1016/j.celrep.2019.11.017.
[34] Majumder B, Baraneedharan U, Thiyagarajan S, Radhakrishnan P, Narasimhan H, Dhandapani M, et al. Predicting clinical response to anticancer drugs using an ex vivo platform that captures tumour heterogeneity. Nat Commun 2015;6:6169. https://doi.org/10.1038/ncomms7169.
[35] Ding Z, Zu S, Gu J. Evaluating the molecule-based prediction of clinical drug responses in cancer. Bioinformatics 2016;32:2891–5. https://doi.org/10.1093/bioinformatics/btw344.
[36] Wingett SW, Andrews S. FastQ Screen: A tool for multi-genome mapping and quality control. F1000Res 2018;7:1338. https://doi.org/10.12688/f1000research.15931.2.
[37] Ewels P, Magnusson M, Lundin S, Käller M. MultiQC: summarize analysis results for multiple tools and samples in a single report. Bioinformatics 2016;32:3047–8. https://doi.org/10.1093/bioinformatics/btw354.
[38] Dobin A, Davis CA, Schlesinger F, Drenkow J, Zaleski C, Jha S, et al. STAR: ultrafast universal RNA-seq aligner. Bioinformatics 2013;29:15–21. https://doi.org/10.1093/bioinformatics/bts635.
[39] Liao Y, Smyth GK, Shi W. featureCounts: an efficient general purpose program for assigning sequence reads to genomic features. Bioinformatics 2014;30:923–30. https://doi.org/10.1093/bioinformatics/btt656.
[40] Pedregosa F, Varoquaux G, Gramfort A, Michel V, Thirion B, Grisel O, et al. Scikit-learn: Machine Learning in Python 2012. https://doi.org/10.48550/ARXIV.1201.0490.
[41] Lin T-Y, Goyal P, Girshick R, He K, Dollár P. Focal Loss for Dense Object Detection 2017. https://doi.org/10.48550/ARXIV.1708.02002.

[42] Kishore J, Goel M, Khanna P. Understanding survival analysis: Kaplan-Meier estimate. Int J Ayurveda Res 2010;1:274. https://doi.org/10.4103/0974-7788.76794.
[43] Harrell FE. Evaluating the Yield of Medical Tests. JAMA 1982;247:2543. https://doi.org/10.1001/jama.1982.03320430047030.
[44] Veličković P, Cucurull G, Casanova A, Romero A, Liò P, Bengio Y. Graph Attention Networks. arXiv:171010903 [Cs, Stat] 2018.
[45] Li Y, Tarlow D, Brockschmidt M, Zemel R. Gated Graph Sequence Neural Networks. arXiv:151105493 [Cs, Stat] 2017.
[46] Luby A, Alves-Guerra M-C. Targeting Metabolism to Control Immune Responses in Cancer and Improve Checkpoint Blockade Immunotherapy. Cancers 2021;13:5912. https://doi.org/10.3390/cancers13235912.
[47] Wang T, Gnanaprakasam JNR, Chen X, Kang S, Xu X, Sun H, et al. Inosine is an alternative carbon source for CD8+-T-cell function under glucose restriction. Nat Metab 2020;2:635–47. https://doi.org/10.1038/s42255-020-0219-4.
[48] Geiger R, Rieckmann JC, Wolf T, Basso C, Feng Y, Fuhrer T, et al. L-Arginine Modulates T Cell Metabolism and Enhances Survival and Anti-tumor Activity. Cell 2016;167:829-842.e13. https://doi.org/10.1016/j.cell.2016.09.031.
[49] Zhao H, Raines LN, Huang SC-C. Carbohydrate and Amino Acid Metabolism as Hallmarks for Innate Immune Cell Activation and Function. Cells 2020;9:562. https://doi.org/10.3390/cells9030562.
[50] Pustylnikov S, Costabile F, Beghi S, Facciabene A. Targeting mitochondria in cancer: current concepts and immunotherapy approaches. Translational Research 2018;202:35–51. https://doi.org/10.1016/j.trsl.2018.07.013.
[51] Huang L, Xu H, Peng G. TLR-mediated metabolic reprogramming in the tumor microenvironment: potential novel strategies for cancer immunotherapy. Cell Mol Immunol 2018;15:428–37. https://doi.org/10.1038/cmi.2018.4.
[52] Aranow C. Vitamin D and the Immune System. Journal of Investigative Medicine 2011;59:881–6. https://doi.org/10.2310/JIM.0b013e31821b8755.
[53] Gong D, Chen M, Wang Y, Shi J, Hou Y. Role of ferroptosis on tumor progression and immunotherapy. Cell Death Discov 2022;8:427. https://doi.org/10.1038/s41420-022-01218-8.
[54] Sprooten J, De Wijngaert P, Vanmeerbeek I, Martin S, Vangheluwe P, Schlenner S, et al. Necroptosis in Immuno-Oncology and Cancer Immunotherapy. Cells 2020;9:1823. https://doi.org/10.3390/cells9081823.
[55] Griffin ME, Hang HC. Microbial mechanisms to improve immune checkpoint blockade responsiveness. Neoplasia 2022;31:100818. https://doi.org/10.1016/j.neo.2022.100818.
[56] Wang X, Geng S. Diet-gut microbial interactions influence cancer immunotherapy. Front Oncol 2023;13:1138362. https://doi.org/10.3389/fonc.2023.1138362.
[57] Melero I, Castanon E, Alvarez M, Champiat S, Marabelle A. Intratumoural administration and tumour tissue targeting of cancer immunotherapies. Nat Rev Clin Oncol 2021;18:558–76. https://doi.org/10.1038/s41571-021-00507-y.
[58] Oster P, Vaillant L, Riva E, McMillan B, Begka C, Truntzer C, et al. *Helicobacter pylori* infection has a detrimental impact on the efficacy of cancer immunotherapies. Gut 2022;71:457–66. https://doi.org/10.1136/gutjnl-2020-323392.
[59] Ostrand-Rosenberg S, Horn LA, Haile ST. The Programmed Death-1 Immune-Suppressive Pathway: Barrier to Antitumor Immunity. The Journal of Immunology 2014;193:3835–41. https://doi.org/10.4049/jimmunol.1401572.
[60] Lemma EY, Letian A, Altorki NK, McGraw TE. Regulation of PD-L1 Trafficking from Synthesis to Degradation. Cancer Immunology Research 2023;11:866–74. https://doi.org/10.1158/2326-6066.CIR-22-0953.

[61] Soltani M, Ghanadian M, Ghezelbash B, Shokouhi A, Zamyatnin AA, Bazhin AV, et al. PD-L1 stimulation can promote proliferation and survival of leukemic cells by influencing glucose and fatty acid metabolism in acute myeloid leukemia. BMC Cancer 2023;23:447. https://doi.org/10.1186/s12885-023-10947-7.
[62] Walker LSK, Sansom DM. Confusing signals: Recent progress in CTLA-4 biology. Trends in Immunology 2015;36:63–70. https://doi.org/10.1016/j.it.2014.12.001.
[63] Qureshi OS, Kaur S, Hou TZ, Jeffery LE, Poulter NS, Briggs Z, et al. Constitutive Clathrin-mediated Endocytosis of CTLA-4 Persists during T Cell Activation. Journal of Biological Chemistry 2012;287:9429–40. https://doi.org/10.1074/jbc.M111.304329.
[64] Curran CS, Gupta S, Sanz I, Sharon E. PD-1 immunobiology in systemic lupus erythematosus. Journal of Autoimmunity 2019;97:1–9. https://doi.org/10.1016/j.jaut.2018.10.025.
[65] Cassady K, Martin PJ, Zeng D. Regulation of GVHD and GVL Activity via PD-L1 Interaction With PD-1 and CD80. Front Immunol 2018;9:3061. https://doi.org/10.3389/fimmu.2018.03061.
[66] Mpakali A, Stratikos E. The Role of Antigen Processing and Presentation in Cancer and the Efficacy of Immune Checkpoint Inhibitor Immunotherapy. Cancers 2021;13:134. https://doi.org/10.3390/cancers13010134.
[67] Lee J, Lozano-Ruiz B, Yang FM, Fan DD, Shen L, González-Navajas JM. The Multifaceted Role of Th1, Th9, and Th17 Cells in Immune Checkpoint Inhibition Therapy. Front Immunol 2021;12:625667. https://doi.org/10.3389/fimmu.2021.625667.
[68] Yang Y, Li X, Ma Z, Wang C, Yang Q, Byrne-Steele M, et al. CTLA-4 expression by B-1a B cells is essential for immune tolerance. Nat Commun 2021;12:525. https://doi.org/10.1038/s41467-020-20874-x.
[69] Durgeau A, Virk Y, Corgnac S, Mami-Chouaib F. Recent Advances in Targeting CD8 T-Cell Immunity for More Effective Cancer Immunotherapy. Front Immunol 2018;9:14. https://doi.org/10.3389/fimmu.2018.00014.
[70] Hanley CJ, Thomas GJ. T-cell tumour exclusion and immunotherapy resistance: a role for CAF targeting. Br J Cancer 2020;123:1353–5. https://doi.org/10.1038/s41416-020-1020-6.
[71] Binnewies M, Roberts EW, Kersten K, Chan V, Fearon DF, Merad M, et al. Understanding the tumor immune microenvironment (TIME) for effective therapy. Nat Med 2018;24:541–50. https://doi.org/10.1038/s41591-018-0014-x.

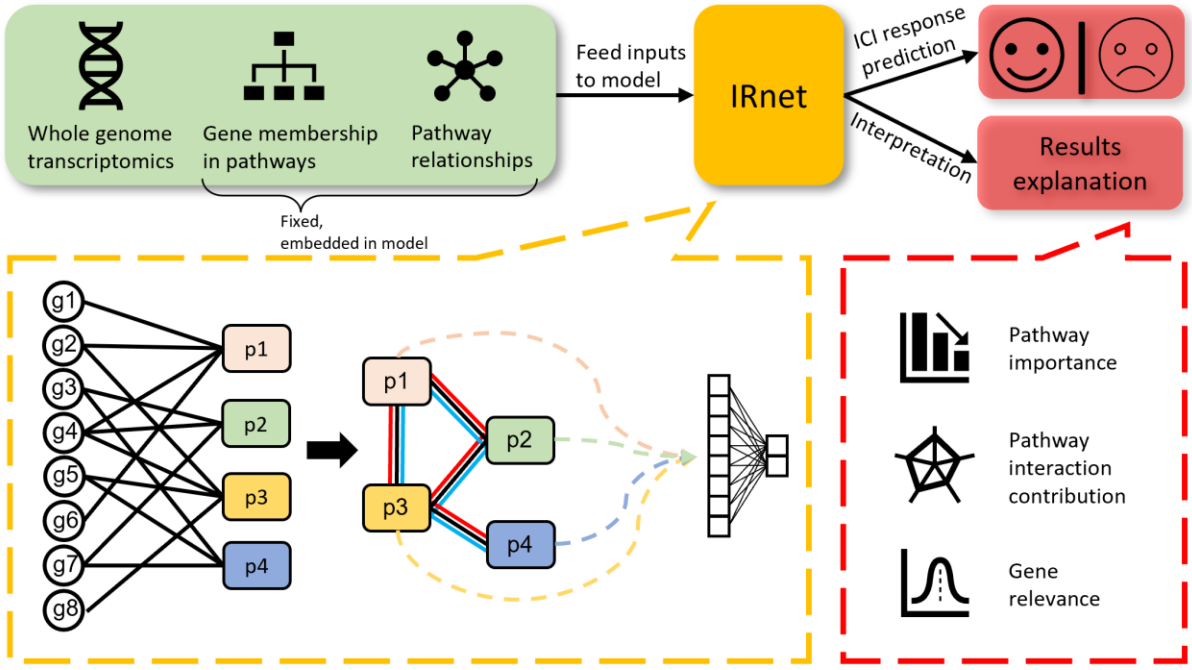

Fig. 1. The workflow of IRnet framework. For training, IRnet takes three types of data/knowledge. For predicting, only the transcriptomics data is needed from users. IRnet provides ICI response prediction, as well as interpretation regarding results. A schematic architecture of IRnet and all three levels of explanation are displayed.

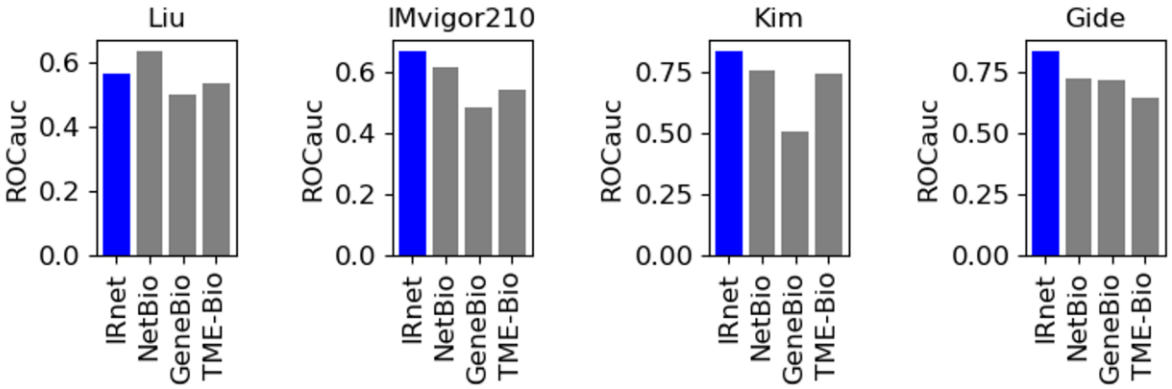

Fig. 2. The within-cohort ICI response prediction performance on different immunotherapy datasets. The performance was measured in terms of the area under the ROC curve.

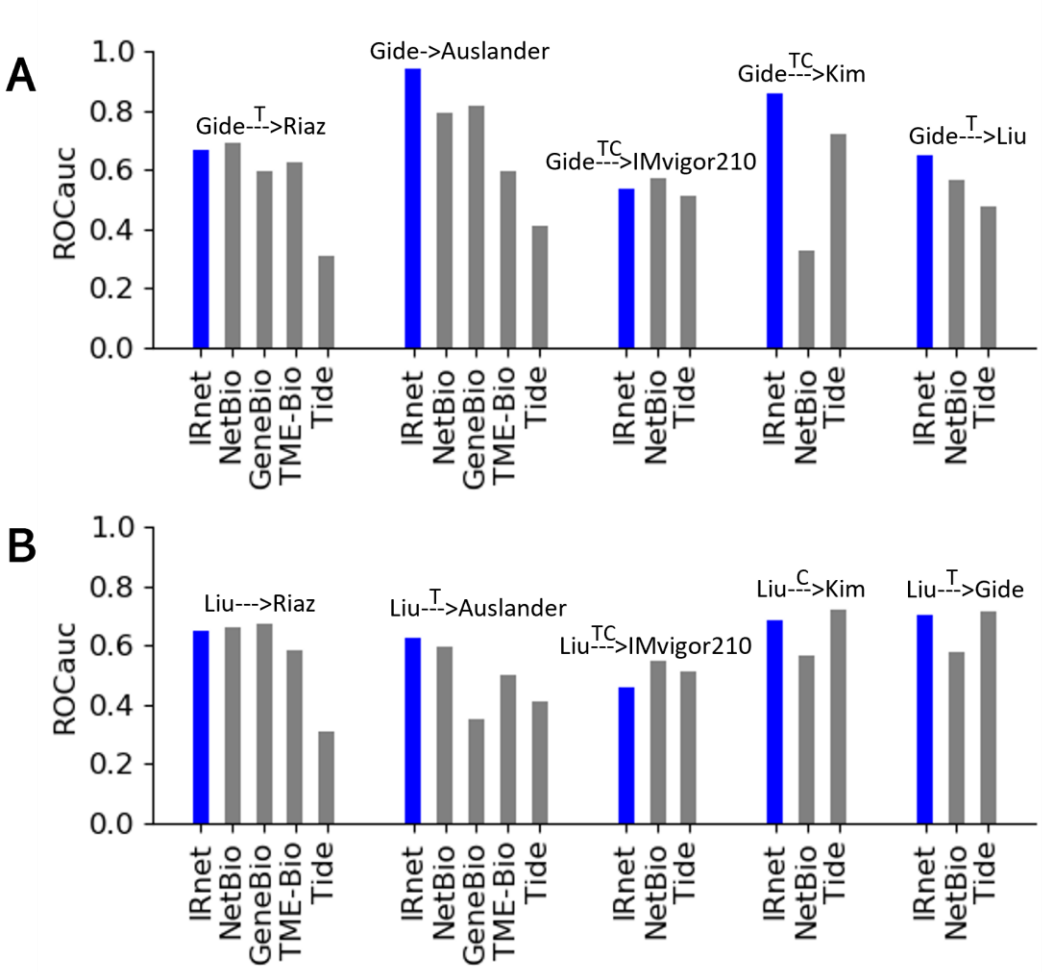

Fig. 3. The cross-cohort ICI response prediction performance by methods trained and tested on different immunotherapy datasets. The performance was measured in terms of the area under the ROC curve. (A) Methods were trained (if possible) on the Gide dataset. (B) Methods were trained (if possible) on the Liu dataset. The "T" mark indicates the ICI treatments are different in the cross-cohort evaluation. The "C" mark indicates the cancer types are different in the cross-cohort evaluation. Note that the specific drug might still be different even though the ICI treatments (ICI targets) are the same.

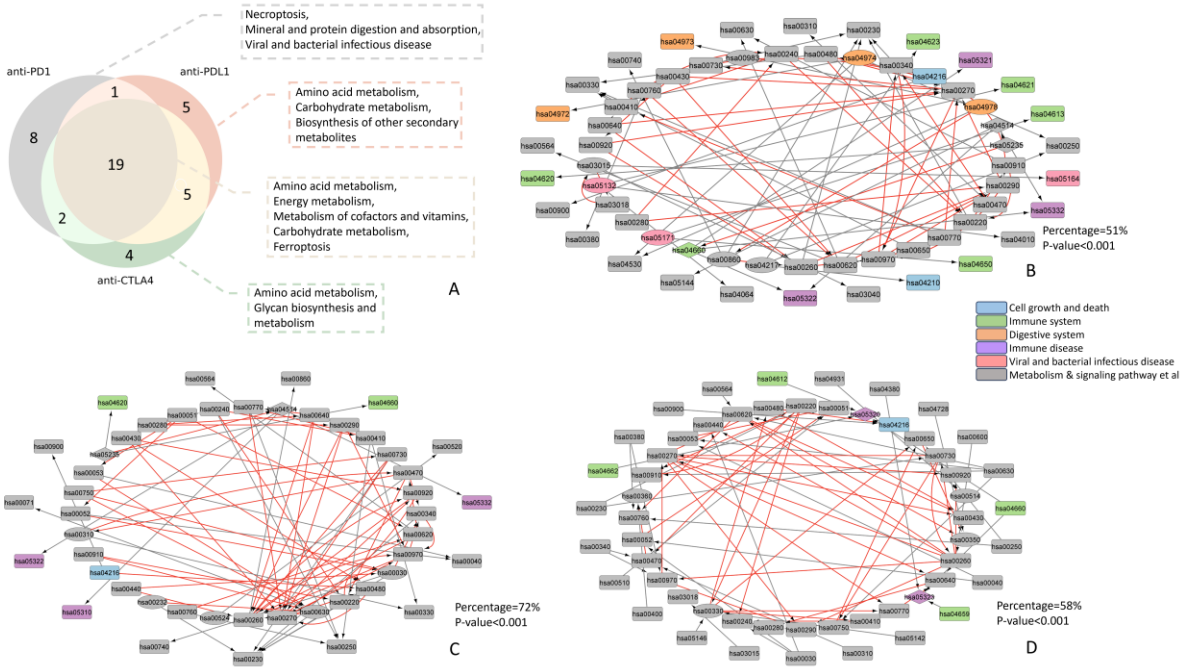

Fig. 4. Pathway-level analysis by IRnet models. (A) The Venn graph shows the interaction between the top 30 ranked pathways from each model. The enriched KEGG pathway categories are marked for the common and unique pathways from different IRnet models. Graphs are constructed by the top 3 ranked interactions (edges) from each of the top 30 pathways (the rectangles in inner circle) and the ICI pathways (the diamonds in inner circle) in (A) anti-PD1 model. (B) anti-PDL1 model. (C) anti-CTLA4 model. An interaction is marked as red color if the target pathway is also among the top 30 ranked pathways. The nodes are filled with colors based on KEGG pathway categories as shown in the legend. The elipse nodes represent pathways that are uniquely top-ranked in the corresponding IRnet model.

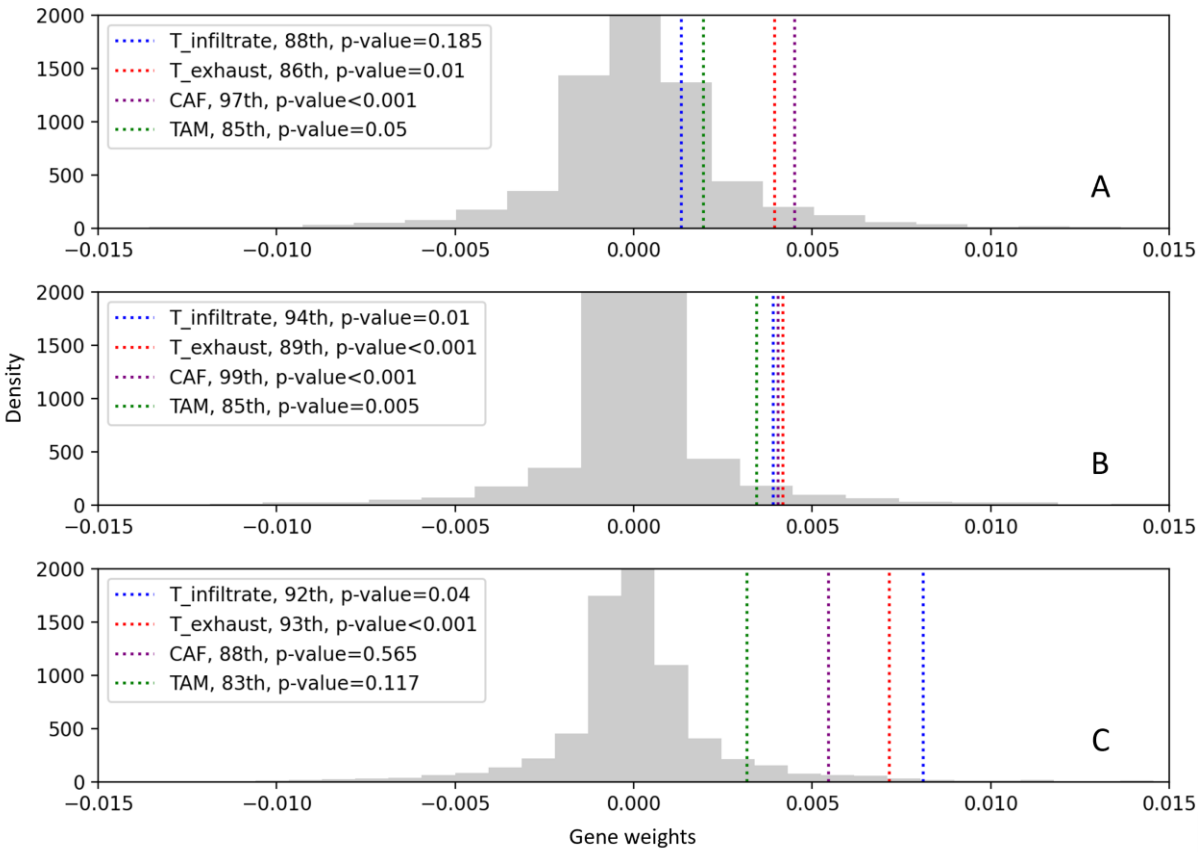

Fig. 5. The distribution of gene weights in (A) anti-PD1 model. (B) anti-PDL1 model. (C) anti-CTLA4 model. The grey histograms represent the counts of genes that fall within the weight bins. The colorful vertical lines indicate the averaged weights of the genes in the corresponding TME marker. The TME marker types, averaged percentiles and their p-values are shown in the legend.

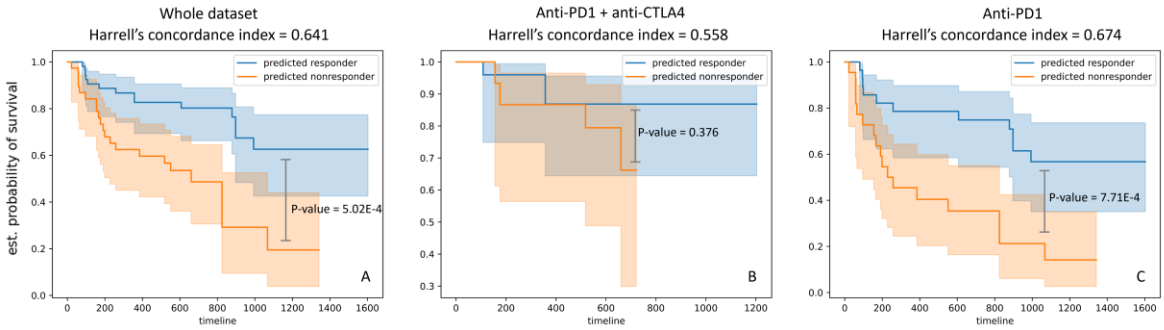

Fig. 6. The estimated survival functions by prediction in (A) the whole Gide dataset. (B) the combination of anti-PD1 and anti-CTLA4 treatment patients in the Gide dataset. (C) the anti-PD1 treatment patients in the Gide dataset.